

1 Towards a Pixel TPC part I: construction and test of a  
2 32 chip GridPix detector

3 M. van Beuzekom<sup>a</sup>, Y. Bilevych<sup>b</sup>, K. Desch<sup>b</sup>, S. van Doesburg<sup>a</sup>,  
4 H. van der Graaf<sup>a</sup>, F. Hartjes<sup>a</sup>, J. Kaminski<sup>b</sup>, P.M. Kluit<sup>a</sup>,  
5 N. van der Kolk<sup>a</sup>, C. Ligtenberg<sup>a</sup>, G. Raven<sup>a</sup>, J. Timmermans<sup>a</sup>

6 <sup>a</sup>*Nikhef, Science Park 105, 1098 XG Amsterdam, The Netherlands*

7 <sup>b</sup>*Physikalisches Institut, University of Bonn, Nussallee 12, 53115 Bonn,*  
8 *Germany*

---

9 **Abstract**

10 A Time Projection Chamber (TPC) module with 32 GridPix chips was con-  
11 structed and the performance was measured using data taken in a testbeam at  
12 DESY in 2021. The GridPix chips each consist of a Timepix3 ASIC (TPX3)  
13 with an integrated amplification grid and have a high efficiency to detect  
14 single ionisation electrons. In the testbeam setup, the module was placed in  
15 between two sets of Mimosas26 silicon detector planes that provided exter-  
16 nal high precision tracking and the whole detector setup was slid into the  
17 PCMAG magnet at DESY. The analysed data were taken at electron beam  
18 momenta of 5 and 6  $GeV/c$  and at magnetic fields of 0 and 1 Tesla(T).

19 The result for the transverse diffusion coefficient  $D_T$  is  $287 \mu m/\sqrt{cm}$  at  
20  $B = 0$  T and  $D_T$  is  $121 \mu m/\sqrt{cm}$  at  $B = 1$  T. The longitudinal diffusion  
21 coefficient  $D_L$  is measured to be  $268 \mu m/\sqrt{cm}$  at  $B = 0$  T and  $252 \mu m/\sqrt{cm}$   
22 at  $B = 1$  T. The diffusion measurements have negligible errors. Results for  
23 the tracking systematical uncertainties in xy (pixel plane) were measured  
24 to be smaller than  $13 \mu m$  with and without magnetic field. The tracking

---

\*Corresponding author, Telephone: +31 20 592 2000  
*Preprint submitted to Nuclear Instruments and Methods A*  
Email address: s01@nikhef.nl (P.M. Kluit)

25 systematical uncertainties in  $z$  (drift direction) were smaller than  $15 \mu\text{m}$  ( $B$   
26  $= 0 \text{ T}$ ) and  $20 \mu\text{m}$  ( $B = 1 \text{ T}$ ).

27 *Keywords:*

28 Micromegas, gaseous pixel detector, micro-pattern gaseous detector,  
29 Timepix, GridPix, pixel time projection chamber

---

## 30 **1. Introduction**

31 Earlier publications on a single chip (1) and four chip (quad) GridPix  
32 detectors (2) showed the potential of the GridPix technology and the large  
33 range of applications for these devices (3). In particular, it was demonstrated  
34 that single ionisation electrons can be detected with high efficiency and great  
35 precision, allowing excellent 3D track position measurements and particle  
36 identification based on the number of electrons and clusters.

37 As a next step towards a Pixel Time Projection Chamber for a future  
38 collider experiment (4), (5), a module consisting of 32 GridPix chips based  
39 on the TPX3 chip was constructed.

40 A GridPix detector consists of a CMOS pixel TPX3 chip (6) with inte-  
41 grated amplification grid added by photolithographic - Micro-electromechanical  
42 Systems (MEMS) - postprocessing techniques. The TPX3 chip can be oper-  
43 ated with a low threshold of  $515 e^-$ , and has a low equivalent noise charge  
44 of about  $70 e^-$ . The GridPix single chip and quad detectors have a very  
45 fine granularity of  $55 \times 55 \mu\text{m}^2$  and a high efficiency to detect single ionisation  
46 electrons.

47 Based on the experience gained with these detectors a 32 GridPix detector  
48 module - consisting of 8 quads - was built. A drift box defining the electric

49 field and gas envelop was constructed. A readout system for up to 128 chips  
50 with 4 multiplexers readout by one Speedy Pixel Detector Readout SPIDR  
51 board (7) (8) was designed. After a series of tests using the laser setup (9)  
52 and cosmics in the laboratory at Nikhef, the detector was taken to DESY for  
53 a two week testbeam campaign.

54 At DESY the 32 chip detector was placed in between two sets of Mimosa26  
55 silicon detector planes and mounted on a movable stage. The whole detector  
56 setup was slid into the centre of the PCMAG magnet at DESY. A beam  
57 trigger was provided by scintillator counters. The data reported here were  
58 taken at different stage positions and electron beam momenta of 5 and 6  
59  $GeV/c$  and at magnetic fields of 0 and 1 T. The performance of the 32  
60 GrixPix detector module was measured using these data sets.

61 In this paper part I of the results will be presented with the main focus  
62 on the detector spatial resolution and tracking performance. A second follow  
63 up paper will discuss the  $dE/dx$  (or  $dN/dx$ ) and other results.

## 64 **2. The 32 GridPix detector module**

65 A 32 GrixPix detector module was built using the quad module (2) as a  
66 basic building block. The quad module consists of four GridPix chips and  
67 is optimised for a high fraction of sensitive area of 68.9%. The external  
68 dimensions are 39.60 x 28.38 mm. The four chips which are mounted on  
69 a cooled base plate (COCA), are connected with wire bonds to a common  
70 central 6 mm wide PCB. A 10 mm wide guard electrode is placed over the  
71 wire bonds 1.1 mm above the aluminium grids, in order to prevent field  
72 distortions of the electric drift field. The guard is the main inactive area,

73 and its dimensions are set by the space required for the wire bonds. On  
74 the back side of the quad module, the PCB is connected to a low voltage  
75 regulator. The aluminium grids of the GridPixes are connected by  $80\ \mu\text{m}$   
76 insulated copper wires to a high voltage (HV) filtering board. The quad  
77 module consumes about 8W of power of which 2W is used in the LV regulator.

78 Eight quad modules were embedded in a box, resulting in a GridPix  
79 detector module with a total of 32 chips. A schematic 3-dimensional drawing  
80 of the detector is shown in Figure 1. A schematic drawing of the quads in  
81 the module is shown in Figure 2, where also the beam direction is indicated.

82 The internal dimensions of the box are 79 mm along the  $x$ -axis, 192 mm  
83 along the  $y$ -axis, and 53 mm along the  $z$ -axis (drift direction), and it has a  
84 maximum drift length (distance between cathode and readout anode) of 40  
85 mm. The drift field is shaped by a series of parallel CuBe field wires of 75  
86  $\mu\text{m}$  diameter with a wire pitch of 2 mm and guard strips are located on all  
87 of the four sides of the active area. In addition, six guard wires - shown with  
88 dashed lines in Figure 2 - are suspended over the boundaries of the chips,  
89 where no guard is present, to minimise distortions of the electric drift field.  
90 The wires are located at a distance of 1.15 mm from the grid planes, and  
91 their potential is set to the drift potential at this drift distance. The box has  
92 two Kapton  $50\ \mu\text{m}$  windows to allow the beam to pass with minimal multiple  
93 scattering.

94 The gas volume of 780 ml is continuously flushed at a rate of  $\sim 50\ \text{ml}/\text{min}$   
95 (about 4 volumes/hour) with premixed T2K TPC gas. This gas is a mixture  
96 consisting of 95% Ar, 3%  $\text{CF}_4$ , and 2%  $\text{iC}_4\text{H}_{10}$  suitable for large TPCs because  
97 of the low transverse diffusion in a magnetic field and the high drift velocity.

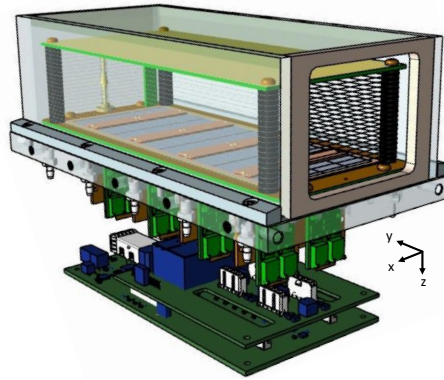


Figure 1: Schematic 3-dimensional render of the 8-quad module detector for illustration purposes.

98 The data acquisition system of the quad module was adopted to allow for  
 99 reading out multiple quads. A multiplexer card was developed that handles  
 100 four quads or 16 chips and combines the TPX3 data into one data stream.  
 101 For the 32 GrixPix module two multiplexers are connected to a SPIDR board

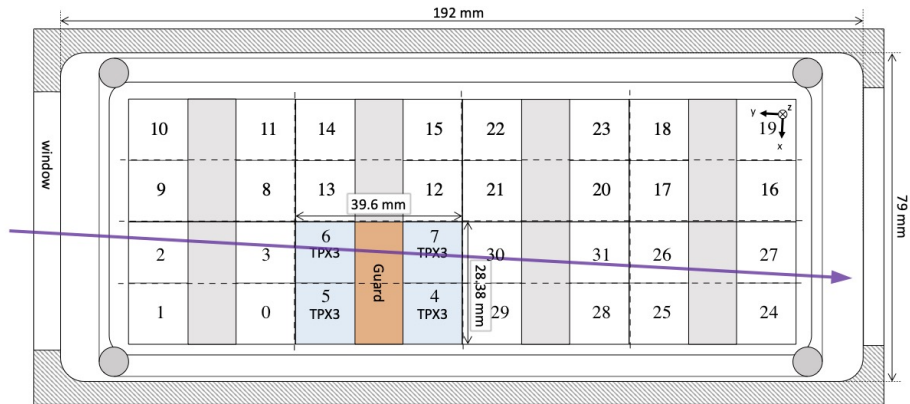


Figure 2: Schematic drawing of the 8-quad module detector with one example quad as viewed from the top of the quads. The chips are numbered and the beam direction is shown in purple.

102 that controls the chips and readout process. The readout speed per chip is  
103 160 Mbps and for the multiplexer 2.56 Gbps this corresponds to a maximum  
104 rate of 21MHits/s. For each pixel the precise Time of Arrival (ToA) using a  
105 640 MHz TDC and the time over threshold (ToT) are measured.

### 106 **3. Experimental setup**

107 In preparation of the two weeks DESY testbeam campaign, a support  
108 frame was designed to move the 32 chip GridPix detector module in the  
109 plane perpendicular to the beam by a remotely controlled stage such that  
110 the whole detector volume could be probed. The module was mounted upside  
111 down with respect to figure 1 to allow access to the electronics from above.  
112 The support frame also held three Mimoso26 silicon detector planes (10) -  
113 with an active area of (21.2 mm x 10.6 mm) - placed in front of the detector  
114 and three Mimoso26 planes behind the detector. At DESY the (Mimoso26)  
115 silicon detector planes were provided by the testbeam coordinators. The  
116 whole detector setup was slided towards the centre of the PCMAG magnet  
117 at the DESY II testbeam facility (10). A beam trigger was provided by  
118 a double scintillator counter coincidence. The data were taken at different  
119 stage positions to cover the whole sensitive TPC volume. Runs with electron  
120 beam momenta of 5 and 6  $GeV/c$  and at magnetic fields of 0 and 1 T were  
121 analysed.

122 A photograph of the detector setup in the PCMAG magnet is shown in  
123 Figure 3.

124 The experimental and environmental parametres such as temperature,  
125 pressure, gas flow, oxyxgen content were measured and logged by a Windows

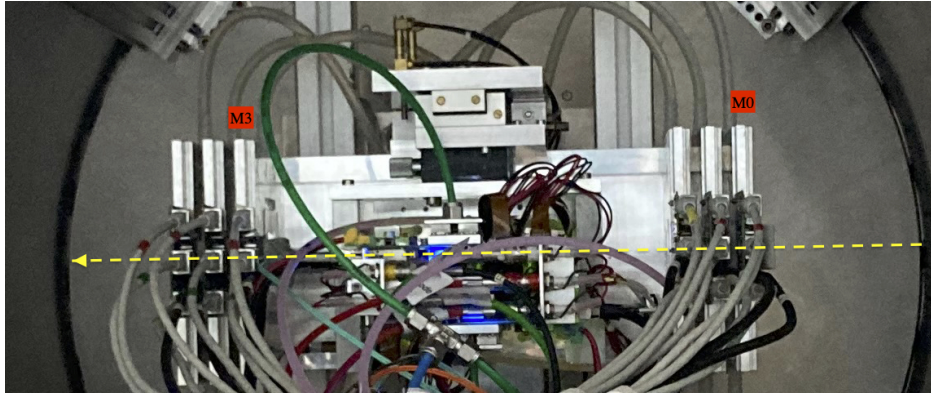


Figure 3: Photo of the detector setup at the centre of the PCMAG magnet. The Mimosa26 planes M0 and M3 are indicated in red as well as the beam direction (yellow). Centrally, the stage positions the TPC module with respect to the beam and the Mimosa26 planes.

126 operated slow control system. The experimental parameters are summarised  
 127 in Table 1. The chips were cooled by circulating Glycol through the cooling  
 128 channels in the module carrier plate. The cooling blocks of the multiplexers  
 129 were further cooled by blowing pressurised air on them.

130 The data was produced in four main data streams: one stream produced  
 131 by the Mimosa26 Telescope, two data streams by the two Timepix multi-  
 132 plexers and one trigger stream. The double scintillator coincidence provided  
 133 a trigger signal to the Trigger Logic Unit (TLU) (11) that sends a signal to  
 134 the telescope readout and the trigger SPIDR. The data acquisition system of  
 135 the Telescope and trigger SPIDR injected a time stamp into their respective  
 136 data streams. Hits from the Mimosa26 planes were collected with a sliding  
 137 window of  $-115 \mu\text{s}$  to  $230 \mu\text{s}$  of the trigger. The data acquisition of the mul-  
 138 tiplexer and the trigger SPIDR were synchronised at the start of the run.  
 139 By comparing the time stamps in these streams, Telescope tracks and TPC

Table 1: Overview of the experimental parameters. The ranges indicate the variation over the data taking period

Number of analysed runs at B=0 (1) T	6 (8)
Run duration	10-90 minutes
Number of triggers per run	3-100 k
$E_{\text{drift}}$	280 V/cm
$V_{\text{grid}}$	340V
Threshold	550 e <sup>-</sup>
Gas temperature	303.3-306.6 K
Pressure	1011 – 1023 mbar
Oxygen concentration	240 - 620 ppm
Water vapour concentration	2000 - 7000 ppm

140 tracks could be matched. Unfortunately, the SPIDR trigger had - due to a  
 141 cabling mistake at the output of the TLU - a common 25ns flat time jitter.

142 After a short data taking period one of the chips (nr 11) developed a  
 143 short circuit and the HV on the grid of the chip was disconnected. After the  
 144 testbeam data taking period the module was repaired in the clean room in  
 145 Bonn.

## 146 4. Analysis

### 147 4.1. Telescope Track reconstruction procedure

148 The data of the Telescope is decoded and analysed using the Corryvreckan  
 149 software package (12). The track model used for fitting was the General  
 150 Broken Lines (GBL) software (14). The code was extended and optimised to



151 fit curved broken lines for the data with magnetic field. The telescope planes  
 152 were iteratively aligned using the standard alignment software provided by  
 153 the package. The single point Mimosas26 resolution is  $4 \mu\text{m}$  in  $x$  and  $6 \mu\text{m}$   
 154 in  $z$  (drift direction) (10).

155 Telescope tracks were selected with at least 5 out of the 6 planes on the  
 156 track and a total  $\chi^2$  of better than 25 per degree of freedom. The uncertain-  
 157 ties on the Telescope track prediction in the middle of the GridPix detector  
 158 module are dominated by multiple scattering. The amount of multiple scat-  
 159 tering was estimated by comparing the predictions from the two telescope  
 160 arms for  $6 \text{ GeV}/c$  tracks at  $B = 0 \text{ T}$ . The expected uncertainty in  $x$  and  $z$  is  
 161  $26 \mu\text{m}$  on average.

#### 162 *4.2. TPC Track reconstruction procedure*

163 GridPx hits are selected requiring a minimum time over threshold ToT  
 164 of  $0.15 \mu\text{s}$ . The drift time is defined as the measured time of arrival minus  
 165 the trigger time recorded in the trigger SPIDR data stream minus a fixed  $t_0$   
 166 (the drift time at zero drift). The drift time was corrected for time walk (2)  
 167 using the measured time over threshold (ToT in units of  $\mu\text{s}$ ) and the formula  
 168 (1):

$$\delta t = \frac{18.6(\text{ns } \mu\text{s})}{\text{ToT} + 0.1577(\mu\text{s})}. \quad (1)$$

169 Furthermore, small time shift corrections - with an odd-even and a  $16 \times 2$   
 170 pixels structure - coming from the TPX3 clock distribution were extracted  
 171 from the data and applied.

172 The  $z$  drift coordinate was calculated as the product of the drift time  
 173 and the drift velocity. This implies that  $z_{\text{drift}} = -z$  as defined in figure 1.

Table 2: Table with track/event selection cuts

Track/Event Selection

$$|x_{\text{TPC}} - x_{\text{Telescope}}| < 0.3 \text{ mm}$$

$$|z_{\text{TPC}} - z_{\text{Telescope}}| < 2 \text{ mm}$$

$$|dx/dy_{\text{TPC}} - dx/dy_{\text{Telescope}}| < 4 \text{ mrad}$$

$$|dz/dy_{\text{TPC}} - dz/dy_{\text{Telescope}}| < 2 \text{ mrad}$$

174 GridPix hits outside an acceptance window of 30 mm wide in x and 15 mm  
 175 wide in z were not used in the track finding and reconstruction. Based on  
 176 a Hough transform an estimate of the TPC track position and angles in the  
 177 middle of the module (at  $y = 1436$  pixels) was obtained. This estimate was  
 178 used to collect the hits around the TPC track and fit the track parameters.  
 179 For this fit a straight line ( $B = 0$  T) or a quadratic track  $B = 1$  T model  
 180 was used. In the fit, the expected uncertainties per hit  $\sigma_x$  and  $\sigma_z$  were used.  
 181 The fit was iterated three times to perform outlier removal at respectively  
 182 10, 5 and 2.5 sigma level. A TPC track was required to have a least 100 hits  
 183 in each multiplexer. At least 25% of the total number of hits should be on  
 184 track and the  $\chi^2$  per degree of freedom had to be less than 3 in xy and zy.  
 185 All track parameters were expressed at a plane in the middle of the TPC.

186 The calibration and alignment of the detector was done using high quality  
 187 tracks for which the track selections are summarised in table 2.

188 The drift velocity was calibrated per run by fitting a linear function to  
 189 the z (predicted from the Telescope track at the measured TPC hit position)  
 190 versus the measured drift time in the TPC. For the  $B = 0$  T runs it varies  
 191 between 61.6 and 63.0  $\mu\text{m}/\text{ns}$ . For the  $B = 1$  T runs it is between 57.2 and

192 59.1  $\mu\text{m}/\text{ns}$ . The variation comes mainly from the changes in the relative  
193 humidity of the gas volume due to small leaks.

194 The individual TPX3 chips were iteratively aligned fitting a shift in x  
195 (z drift) and two slopes  $dx(z \text{ drift})/d \text{ row}(\text{column})$ . The alignment was done  
196 per run, because the detector was moved in x and/or z for each run. The  
197 fitted slopes were also corrected for small shifts and rotations (3D) in the  
198 nominal chip position.

199 An example event run 6916 without B field with a TPC and a telescope  
200 track is shown in figure 4. The TPC is located between  $y = 0$  and 2872  
201 pixels. Three Mimosas26 planes are located at  $y < -1000$  and three at  $y >$   
202 4000 pixels.

## 203 5. Hit resolutions

204 In order to study the single electron resolution for the data with and  
205 without magnetic field, additional selections on the Telescope and TPC tracks  
206 were applied. Due to the trigger time jitter of 25 ns (corresponding to 1.5  
207 mm drift), the prediction of the telescope track in z must be used as the  
208 reference for z. Secondly, the z hits of the TPC track were fitted to correct  
209 for the common time shift and the z residuals were calculated with respect to  
210 the fitted TPC track. In the xy plane the residuals of TPC hits with respect  
211 to the telescope track were used to extract the single electron resolution in  
212 xy. For the resolution studies runs at three different z stage positions of the  
213 TPC were selected where the beam gave hits in the central chips. The data  
214 of 14 central chips (9, 12, 21, 20, 17, 16, 2, 3, 6, 7, 30, 31, 26 and 27) was  
215 used. Two chips (8 and 13) were left out because of the E field deformations

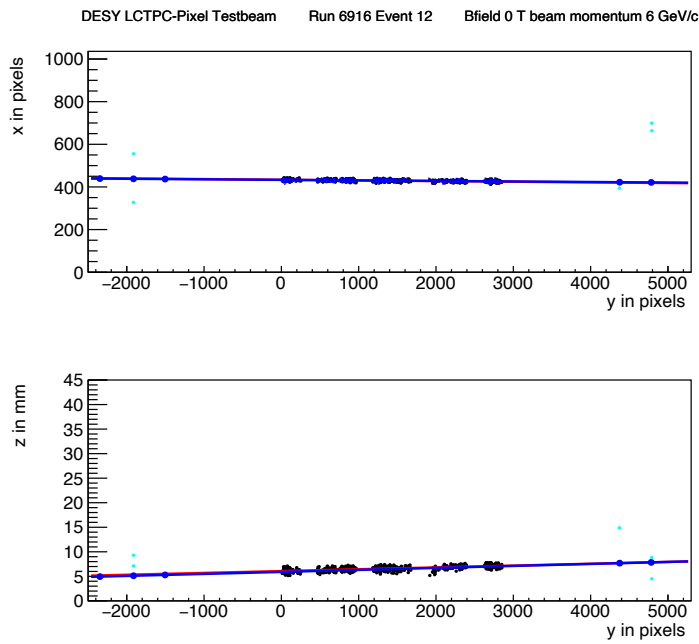


Figure 4: An event display for run 6916 without B field, with in total 1293 TPC hits (black dots) in the precision plane ( $x,y$ ) and driftplane ( $z$  drift, $y$ ). The fitted TPC track (red line) with 1130 hits on track and the telescope track (blue line) with 5 Mimoso26 planes (blue hits) on track are shown. In green the off track Mimoso26 hits are shown.

216 caused by the short circuit in chip 11.

### 217 5.1. Hit resolutions in the pixel plane

218 The resolution of the hits in the pixel plane ( $xy$ ) was measured as a  
219 function of the predicted drift position ( $z_{\text{drift}}$ ). Only hits are used crossing  
220 the fiducial region defined by the central core of the beam and staying 20  
221 pixels away from the chip edges. The resolution for the detection of ionisation  
222 electrons  $\sigma_x$  is given by:

$$\sigma_x^2 = \frac{d_{\text{pixel}}^2}{12} + d_{\text{track}}^2 + D_T^2(z_{\text{drift}} - z_0), \quad (2)$$

223 where  $d_{\text{pixel}}$  is the pixel pitch size,  $d_{\text{track}}$  the uncertainty from the track pre-  
224 diction,  $z_0$  is the position of the grid, and  $D_T$  is the transverse diffusion  
225 coefficient. The resolution at zero drift distance  $d_{\text{pixel}}/\sqrt{12}$  was fixed to 15.9  
226  $\mu\text{m}$  and  $d_{\text{track}}$  to 30  $\mu\text{m}$  for  $B = 0$  T and 42  $\mu\text{m}$  for  $B = 1$  T data. The  
227 uncertainty of the track prediction was measured and is larger than the Mi-  
228 mosa plane resolution because of multiple scattering in the sensor and in the  
229 entrance and exit windows.

230 The expression (2) - leaving  $z_0$  and  $D_T$  as free parameters - is fitted to  
231 the  $B = 0$  T data shown in Figure 5. The fit gives a transverse diffusion  
232 coefficient  $D_T$  of 287  $\mu\text{m}/\sqrt{\text{cm}}$  with negligible statistical uncertainty. The  
233 measured value is in agreement with the value of 287  $\mu\text{m}/\sqrt{\text{cm}} \pm 4\%$  pre-  
234 dicted by the gas simulation software Magboltz 11.9 (15). The values of the  
235 diffusion coefficients depend on the humidity that was not precisely mea-  
236 sured during the testbeam. The humidity strongly affects the drift velocity.  
237 Therefore the drift velocity prediction from Magboltz was used to determine

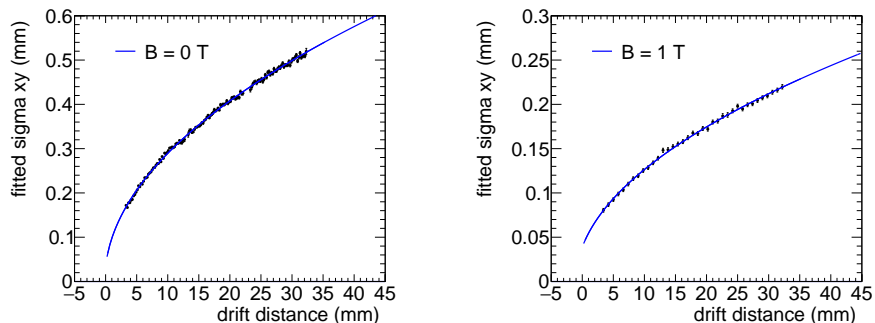


Figure 5: Measured hit resolution in the pixel plane (black points) fitted with the resolution function according to equation (2) (blue line).

238 the water content per run and predictions for the diffusion coefficients could  
 239 be obtained.

240 A fit to the  $B = 1$  T data, also shown in Figure 5, gives a transverse dif-  
 241 fusion coefficient  $D_T$  of  $121 \mu\text{m}/\sqrt{\text{cm}}$  with negligible statistical uncertainty.  
 242 The measured value is in agreement with the value of  $119 \mu\text{m}/\sqrt{\text{cm}} \pm 2\%$   
 243 predicted by Magboltz.

### 244 5.2. Hit resolution in the drift plane

245 The resolution for the detection of ionisation electrons  $\sigma_z$  in the drift  
 246 plane is given by:

$$\sigma_z^2 = \sigma_{z0}^2 + d_{\text{track}}^2 + D_L^2(z_{\text{drift}} - z_0), \quad (3)$$

247 where  $\sigma_{z0}$  is the resolution at zero drift distance,  $d_{\text{track}}$  the expected track  
 248 uncertainty and  $D_L$  the longitudinal diffusion constant. Only tracks crossing  
 249 the fiducial region were accepted and hits with a ToT value above  $0.6 \mu\text{s}$   
 250 were selected. Because of the time jitter, the fitted TPC track is used for the

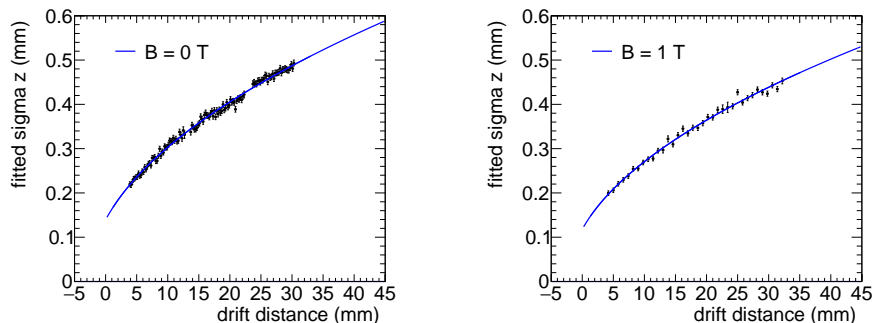


Figure 6: Resolution in the drift plane for hits with a ToT above  $0.60 \mu\text{s}$ . The data are fitted with the expression of equation (3).

251 drift residuals. For  $z_{\text{drift}}$  the Telescope prediction at the hit was used. The  
 252 expected uncertainty on the Telescope track prediction is  $25 \mu\text{m}$ .

253 The expression (3) - leaving  $\sigma_{z_0}$  and  $D_L$  as free parameters - is fitted  
 254 to the  $B = 0 \text{ T}$  data shown in Figure 6. The value of  $z_0$  was fixed to the  
 255 result of the fit in the  $xy$  plane. The value of  $\sigma_{z_0}$  was measured to be  $138$   
 256  $\mu\text{m}$ . The longitudinal diffusion coefficient  $D_L$  was determined to be  $(265 \pm$   
 257  $1) \mu\text{m}/\sqrt{\text{cm}}$ , which is higher than the expected value  $(236 \pm 3) \mu\text{m}/\sqrt{\text{cm}}$   
 258 from a Magboltz calculation (15).

259 A fit to the  $B = 1 \text{ T}$  data shown in Figure 6 gives a longitudinal diffusion  
 260 coefficient  $D_L$  of  $(250 \pm 2) \mu\text{m}/\sqrt{\text{cm}}$ . The measured value is in agreement  
 261 with the value of  $(245 \pm 4) \mu\text{m}/\sqrt{\text{cm}}$  predicted by Magboltz. The fitted  
 262 value of  $\sigma_{z_0}$  was  $133 \mu\text{m}$ .

### 263 5.3. Deformations in the pixel and drift plane

264 It is important to measure possible deformations in the pixel ( $xy$ ) and  
 265 drift ( $z$ ) plane to quantify the tracking precision. For the construction of

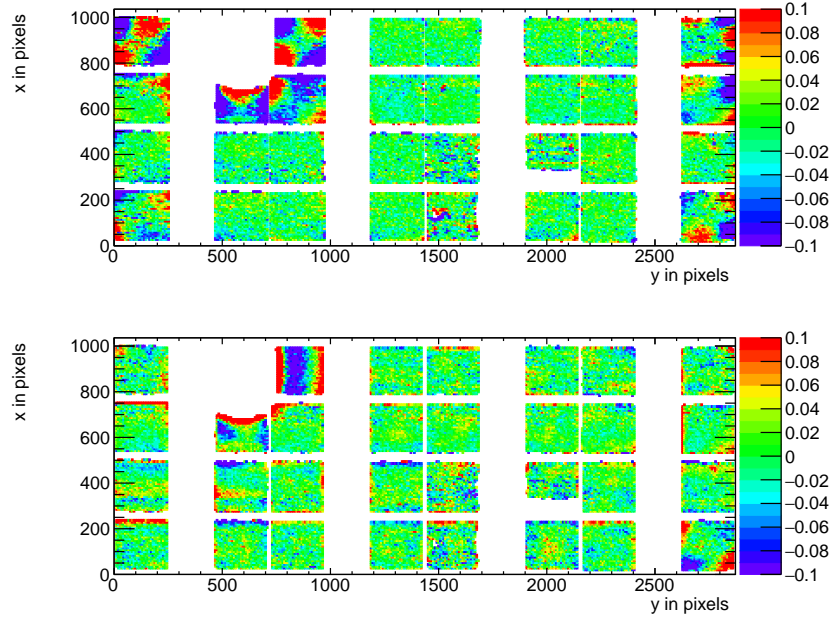


Figure 7: Mean residuals (in mm) in the pixel (top) and drift (bottom) plane for  $B = 0$  T data at the expected hit position.

266 a large Pixel TPC, deformations in the pixel plane deformation should be  
 267 controlled to better than typically  $20 \mu\text{m}$  because these affect the momentum  
 268 resolution. The mean residuals in the pixel and drift planes are shown in  
 269 Figure 7 for the  $B = 0$  T data set using a large set of runs to cover the whole  
 270 module. The residuals were calculated with respect to the Telescope track  
 271 prediction. Because of limited statistics bins were grouped into  $8 \times 16$  pixels.  
 272 Bins with less than 100 hits are left out and residuals larger (smaller) than  
 273  $+(-)100 \mu\text{m}$  are shown in red (blue).

274 A few critical areas can be observed in figure 7: the region around chip 11  
 275 is affected (chips 14, 8 and 13), because the grid of chip 11 was disconnected.  
 276 Deformations are present at the four corners of the drift box (chips 1, 10, 19



277 and 24) and close to the upper corner edge (chip 16) of the drift box. These  
278 come from inhomogenities in the drift field near the supporting pillars, the  
279 field wires are too close to the chip to provide a constant electric field. It  
280 was concluded that for the deformation results the hits of these nine chips  
281 have to be removed. The track fit was redone leaving these hits out of the  
282 fit, such that they could not bias and affect the results.

283 In order to reduce the statistical fluctuations and quantify the tracking  
284 precision, the module was regrouped in four 256x256 pixel planes put side by  
285 side on the horizontal axis, as shown in figure 8. Bins have a size of 16x16  
286 pixels and bins with less than 1000 entries are not shown. A bias in the  
287 mean residual at the edge of the chips is expected to be present for an ideal  
288 detector because of the finite coverage and the diffusion in the drift process.  
289 Due to the presence of the dike pixels at the edge of the chip became covered  
290 and inefficient. Therefore the region near the edge of 5 pixels was removed.  
291 For the drift coordinate a region of 10 pixels was removed. The total number  
292 of measurements (bins) in xy is 895 and in z 892. One can observe that in the  
293 module plane no clear systematic deviations are present and conclude that  
294 the guard wire voltages were on average well tuned. Note that in the quad  
295 module we had no guard wires and deformation corrections had to be applied  
296 (2). The r.m.s. of the distribution of the measured mean residual over the  
297 surface in the pixel plane is 11  $\mu\text{m}$  and in the drift plane 15  $\mu\text{m}$ . Similarly,  
298 regrouping the module in four planes of 256x256 pixels putting them on top  
299 of each other vertically, yielded a r.m.s. in the pixel plane of 13  $\mu\text{m}$  and 13  
300  $\mu\text{m}$  in the drift coordinate. The expected statistical error in xy is 4  $\mu\text{m}$  and  
301 in z 5  $\mu\text{m}$ .

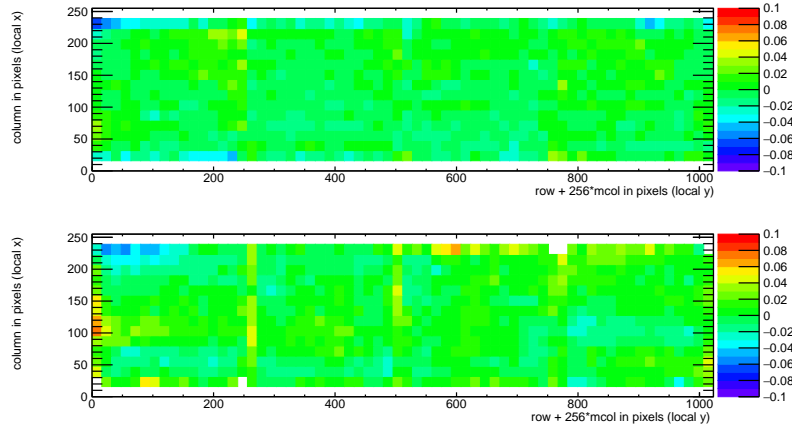


Figure 8: Mean residuals (in mm) in the pixel (top) and drift plane (bottom) for  $B = 0$  T data at the regrouped expected hit position.

302 In the  $B = 1$  T data set, the electrons will drift mainly along the magnetic  
 303 field lines. Deformations are in that case due to e.g. the non-alignment of the  
 304 electric and magnetic field, giving ExB effects. Unfortunately, the statistics  
 305 of the Telescope tracks that have a matched TPC track was insufficient and  
 306 did not cover the full TPC module plane. Therefore the larger statistics of  
 307 matched and unmatched TPC tracks was used. TPC tracks were required  
 308 to pass angular selection cuts ( $dx/dy$  between -40 and -20 mrad and  $dz/dy$   
 309 between 0 and 14 mrad) and a momentum cut ( $p > 2$  GeV/c and  $q < 0$ ).

310 The mean residuals in the pixel and drift planes are shown in figure 9 for  
 311 the  $B = 1$  T data set using a large set of runs to cover the whole module. The  
 312 residuals were calculated with respect to the TPC track prediction. Because  
 313 of limited statistics bins were grouped into  $8 \times 16$  pixels. Bins with less than  
 314 100 hits are left out and residuals larger (smaller) than  $+(-)100 \mu\text{m}$  are shown  
 315 in red (blue).

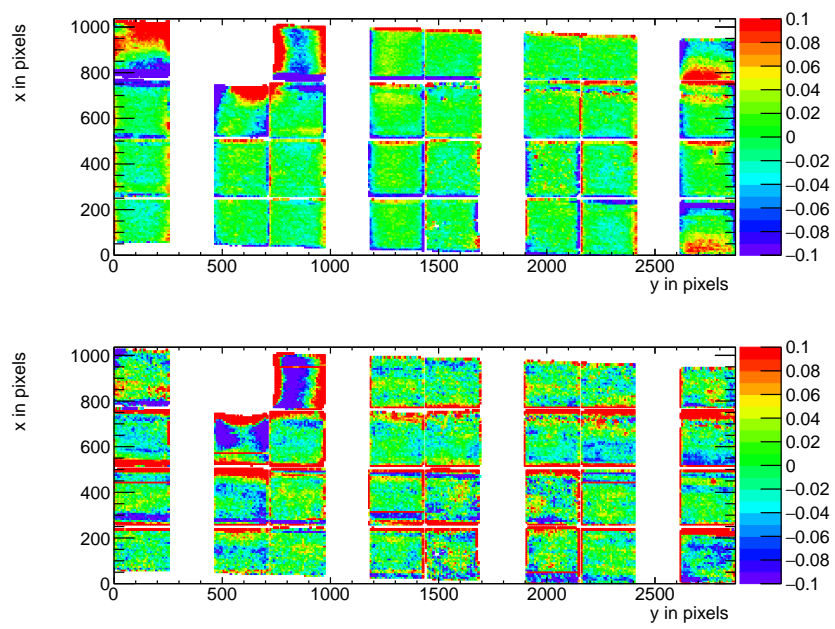


Figure 9: Mean residuals in the pixel and drift plane for  $B = 1$  T data at the expected hit position.

316 In figure 9 the critical areas discussed above - around chip 11, the four  
317 corner chips and chip 16 in the upper corner edge - can be clearly observed.  
318 For the deformation results the hits of these nine chips have to be removed.  
319 The TPC track fit was redone leaving these hits out of the fit, thus that  
320 they could not bias and affect the results. The TPC plane is well covered,  
321 although one can observe that due to the angle of the beam in the xy plane  
322 the chips in the upper right and lower left corners are not fully covered.

323 In order to reduce the statistical fluctuations and quantify the tracking  
324 precision, the module was regrouped in four 256x256 pixel planes put side by  
325 side on the horizontal axis, as shown in figure 10. Bins have a size of 16x16  
326 pixels and bins with less than 1000 entries are not shown. Similar to the  
327 no-field deformations studies, acceptance cuts had to be applied. The region  
328 near the edge of 16 pixels (columns) was removed. For the drift coordinate  
329 in addition a region of 10 pixels (rows) was removed. The total number of  
330 measurements (bins) in xy is 896 and in z 896. One can observe that in  
331 the module plane no clear systematic deviations are present. The r.m.s. of  
332 the distribution of the measured mean residual over the surface in the pixel  
333 plane is 13  $\mu\text{m}$  and in the drift plane 19  $\mu\text{m}$ . Similarly, regrouping the module  
334 in four planes of 256x256 pixels side by side vertically, yielded a r.m.s. in  
335 the pixel plane of 11  $\mu\text{m}$  and 20  $\mu\text{m}$  in the drift coordinate. The expected  
336 statistical error in xy is 2  $\mu\text{m}$  and in z 3  $\mu\text{m}$ .

#### 337 5.4. Tracking resolution

338 A selected TPC track in the  $B = 0$  T data has on average 1000 hits. The  
339 tracking precision in the middle of the TPC was derived on a track-by-track  
340 bias and found to be on average 9  $\mu\text{m}$  in the precision plane and 13  $\mu\text{m}$

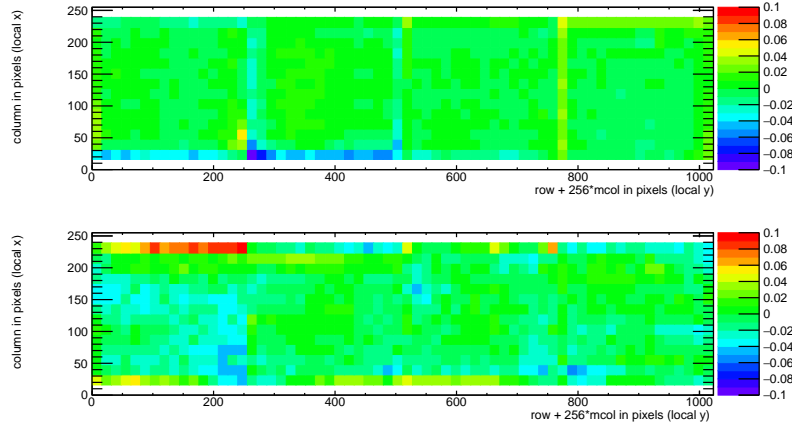


Figure 10: Mean residuals in the pixel and drift plane for  $B=1\text{T}$  data at the regrouped expected hit position.

341 in  $z$ . The angular resolution in  $dx/dy$  was on average  $0.19$  mrad and for  
 342  $dz/dy$   $0.25$  mrad. It is clear that the position resolution in the TPC in the  
 343 precision and drift coordinates is impressive for a track length of (only)  $158$   
 344 mm. The values are smaller than the uncertainty on the track prediction  
 345 from the silicon telescope of  $26\ \mu\text{m}$  on average that is dominated by multiple  
 346 scattering.

## 347 6. Single electron efficiency

348 The distribution of the number of TPC track hits per chip - without  
 349 requiring a matched Telescope track - are shown in figure 11 for the data  
 350 without magnetic field and for the  $B = 1\ \text{T}$  data. The  $B = 0\ \text{T}$  data analysis  
 351 selects the central chips 2,6,7,9,16,17,26 and 27. The  $B = 1\ \text{T}$  data analysis  
 352 selects the same chips plus chips 12,13,20 and 21.

353 The mean number of hits is measured to be  $124$  and  $89$  in the  $B = 0\ \text{T}$

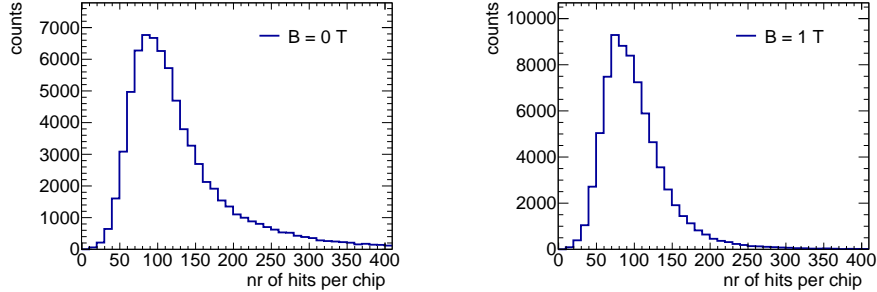


Figure 11: Distribution of the number of track hits per per chip for  $B = 0$  T (left)  $B = 1$  T data.

354 and 1 T data sets respectively. The most probable values are respectively  
 355 87 and 64. Note that the  $B = 0$  T data have a much larger Landau-like tail  
 356 than the 1 T data. Also the fluctuations in the core of the distribution are  
 357 larger. The mean time over threshold is  $0.68 \mu\text{s}$  for the  $B = 0$  T and  $0.86$   
 358  $\mu\text{s}$  at a  $B = 1$  T data. This means that the deposited charge per pixel is  
 359 smaller for the 0 T data. The most probable value for the total deposited  
 360 charge is similar for both data sets. A possible explanation for this behavior  
 361 is that because of the reduced transverse diffusion in the  $B = 1$  T data, the  
 362 possiblility of two primary electrons ending up in a single grid hole is higher.  
 363 The mean number of hits is in agreement with the predictions of (13) 106  
 364 electron-ion pairs for a  $6 \text{ GeV}/c$  electron at  $B = 0$  T, crossing 236 pixels or  
 365 12.98 mm and a detector running at 85% single electron efficiency.

## 366 7. Conclusion and outlook

367 A Time Projection Chamber module with 32 GridPix chips was con-  
 368 structed and the performance was measured using data taken in a testbeam

369 at DESY in 2021. The analysed data were taken at electron beam momenta  
370 of 5 and 6  $GeV/c$  and at magnetic fields of 0 and 1 T.

371 The result for the transverse diffusion coefficient  $D_T$  is  $287 \mu\text{m}/\sqrt{cm}$  at  
372  $B = 0$  T and  $D_T$  is  $121 \mu\text{m}/\sqrt{cm}$  at  $B = 1$  T. The longitudinal diffusion  
373 coefficient  $D_L$  is measured to be  $268 \mu\text{m}/\sqrt{cm}$  at  $B = 0$  T and  $252 \mu\text{m}/\sqrt{cm}$   
374 at  $B = 1$  T. Results for the tracking systematical uncertainties in xy were  
375 measured to be smaller than  $13 \mu\text{m}$  with and without magnetic field. The  
376 tracking systematical uncertainties in z were smaller than  $15 \mu\text{m}$  ( $B = 0$  T)  
377 and  $20 \mu\text{m}$  ( $B = 1$  T).

378 The mean number of hits is in agreement with the predictions of (13) and  
379 a detector running at 85% single electron efficiency.

380 Not all data were analysed and users are welcome to study them using  
381 the data sets on available on the Grid.

382 The GridPix detector will be further tested and developed in view of a  
383 TPC that will be installed in a heavy ion experiment at the EIC or other  
384 future colliders. A follow up paper is in preparation on the measured  $dE/dx$   
385 or  $dN/dx$  resolution and other performance topics.

## 386 **Acknowledgements**

387 This research was funded by the Netherlands Organisation for Scientific  
388 Research NWO. The authors want to thank the support of the mechanical  
389 and electronics departments at Nikhef and the detector laboratory in Bonn.  
390 The measurements leading to these results have been performed at the Test  
391 Beam Facility at DESY Hamburg (Germany), a member of the Helmholtz  
392 Association (HGF).

393 **References**

394 [1] C. Ligtenberg, et al., Performance of a GridPix detector based  
395 on the Timepix3 chip, Nucl. Instrum. Meth. A 908 (2018) 18–23.  
396 arXiv:1808.04565, doi:10.1016/j.nima.2018.08.012.

397 [2] C. Ligtenberg, et al., Performance of the GridPix detector quad,  
398 Nucl. Instrum. Meth. A 956 (2020) 163331. arXiv:2001.01540,  
399 doi:10.1016/j.nima.2019.163331.

400 [3] J. Kaminski, Y. Bilevych, K. Desch, C. Krieger, M. Lupberger, GridPix  
401 detectors - introduction and applications, Nucl. Instrum. Meth. A845  
402 (2017) 233–235. doi:10.1016/j.nima.2016.05.134.

403 [4] C. Ligtenberg, A GridPix TPC readout for the ILD experiment at the  
404 future International Linear Collider, Ph.D. thesis, Free University of  
405 Amsterdam (2021).

406 URL [https://www.nikhef.nl/pub/services/biblio/theses\\_pdf/thesis\\_C.Ligtenberg.p](https://www.nikhef.nl/pub/services/biblio/theses_pdf/thesis_C.Ligtenberg.p)

407 [5] M. Lupberger, Y. Bilevych, H. Blank, D. Danilov, K. Desch, A. Hamann,  
408 J. Kaminski, W. Ockenfels, J. Tomtschak, S. Zigann-Wack, To-  
409 ward the Pixel-TPC: Construction and Operation of a Large Area  
410 GridPix Detector, IEEE Trans. Nucl. Sci. 64 (5) (2017) 1159–1167.  
411 doi:10.1109/TNS.2017.2689244.

412 [6] T. Poikela, J. Plosila, T. Westerlund, M. Campbell, M. De Gaspari,  
413 X. Llopart, V. Gromov, R. Kluit, M. van Beuzekom, F. Zappone,  
414 V. Zivkovic, C. Brezina, K. Desch, Y. Fu, A. Kruth, Timepix3: a  
415 65K channel hybrid pixel readout chip with simultaneous ToA/ToT and



- 416 sparse readout, JINST 9 (05) (2014) C05013.  
417 URL <http://stacks.iop.org/1748-0221/9/i=05/a=C05013>
- 418 [7] J. Visser, M. van Beuzekom, H. Boterenbrood, B. van der Heijden, J. I.  
419 Muñoz, S. Kulis, B. Munneke, F. Schreuder, SPIDR: a read-out system  
420 for Medipix3 & Timepix3, Journal of Instrumentation 10 (12) (2015)  
421 C12028. doi:10.1088/1748-0221/10/12/C12028.
- 422 [8] B. van der Heijden, J. Visser, M. van Beuzekom, H. Boterenbrood,  
423 S. Kulis, B. Munneke, F. Schreuder, SPIDR, a general-purpose readout  
424 system for pixel ASICs, JINST 12 (02) (2017) C02040. doi:10.1088/1748-  
425 0221/12/02/C02040.
- 426 [9] F. Hartjes, A diffraction limited nitrogen laser for detector calibration  
427 in high energy physics, Ph.D. thesis, University of Amsterdam (1990).  
428 URL [https://www.nikhef.nl/pub/services/biblio/theses\\_pdf/thesis\\_F\\_Hartjes.pdf](https://www.nikhef.nl/pub/services/biblio/theses_pdf/thesis_F_Hartjes.pdf)
- 429 [10] R. Diener et al., The DESY II test beam facility, Nuclear Instru-  
430 ments and Methods in Physics Research. Section A: Accelerators, Spec-  
431 trometers, Detectors and Associated Equipment 922 (2019) 265–286.  
432 arXiv:1807.09328, doi:10.1016/j.nima.2018.11.133.
- 433 [11] P. Baesso, D. Cussans, J. Goldstein, , Journal of Instrumentation 14 (09)  
434 (2019) P09019–P09019. arXiv:2005.00310.  
435 URL <https://doi.org/10.1088/1748-0221/14/09/p09019>
- 436 [12] D. Dannheim, K. Dort, L. Huth, D. Hynds, I. Kremastiotis, J. Kröger,  
437 M. Munker, F. Pitters, P. Schütze, S. Spannagel, T. Vanat, M. Williams,

- 438 , Journal of Instrumentation 16 (03) (2021) P03008. doi:10.1088/1748-  
439 0221/16/03/p03008. arXiv:2011.12730.  
440 URL <https://doi.org/10.1088/1748-0221/16/03/p03008>
- 441 [13] R. Veenhof, Garfield - simulation of gaseous detectors, version 9, Refer-  
442 ence W5050 (1984-2010).  
443 URL <https://garfield.web.cern.ch>
- 444 [14] C. Kleinwort, General broken lines as advanced track fitting method,  
445 Nuclear Instruments and Methods in Physics Research Section A: Accel-  
446 erators, Spectrometers, Detectors and Associated Equipment 673 (2012)  
447 107–110. doi:10.1016/j.nima.2012.01.024.
- 448 [15] S. F. Biagi, Monte Carlo simulation of electron drift and diffusion  
449 in counting gases under the influence of electric and magnetic fields,  
450 Nucl. Instrum. Meth. A421 (1-2) (1999) 234–240. doi:10.1016/S0168-  
451 9002(98)01233-9.  
452 URL <https://magboltz.web.cern.ch/magboltz>